Mon. Not. R. Astron. Soc. **000**, 000–000 (0000) Printed 1 February 2008 (MN LATEX style file v2.2)

Line Emission in the Brightest Cluster Galaxies of the NOAO Fundamental Plane and Sloan Digital Sky Surveys

Louise O.V. Edwards[1], Michael J. Hudson[2], Michael L. Balogh[2], Russell J. Smith[3]
[1] *Département de Physique, Génie Physique et d'Optique, Université Laval and Observatoire du mont Mégantic, Québec, QC, G1K 7P4, Canada*
[2] *Department of Physics and Astronomy, University of Waterloo, Waterloo, ON, N2L 3G1, Canada*
[3] *Department of Physics, Durham University, Durham UK,DH1 3LE*

arXiv:0704.3242v1 [astro-ph] 24 Apr 2007

1 February 2008

ABSTRACT

We examine the optical emission line properties of Brightest Cluster Galaxies (BCGs) selected from two large, homogeneous datasets. The first is the X-ray selected National Optical Astronomy Observatory Fundamental Plane Survey (NFPS), and the second is the C4 catalogue of optically selected clusters built from the Sloan Digital Sky Survey Data Release 3 (SDSS DR3). Our goal is to better understand the optical line emission in BCGs with respect to properties of the galaxy and the host cluster. Throughout the analysis we compare the line emission of the BCGs to that of a control sample made of the other bright galaxies near the cluster centre. Overall, both the NFPS and SDSS show a modest fraction of BCGs with emission lines ($\sim 15\%$). No trend in the fraction of emitting BCGs as a function of galaxy mass or cluster velocity dispersion is found. However we find that, for those BCGs found in cooling flow clusters, 71^{+9}_{-14} have optical emission. Furthermore, if we consider only BCGs within 50kpc of the X-ray centre of a cooling flow cluster, the emission-line fraction rises further to 100^{+0}_{-15} %. Excluding the cooling flow clusters, only $\sim$ 10 % of BCGs are line emitting, comparable to the control sample of galaxies. We show that the physical origin of the emission line activity varies: in some cases it has LINER-like line ratios, whereas in others it is a composite of star-formation and LINER-like activity. We conclude that the presence of emission lines in BCGs is directly related to the cooling of X-ray gas at the cluster centre.

Key words: galaxies: clusters, cooling flows:general – galaxies: evolution – stars: formation – galaxies: stellar content – surveys

1 INTRODUCTION

The brightest cluster galaxy (BCG) is typically a giant, red elliptical or cD galaxy, located near the centre of the gravitational potential. It is likely that a rich history of galaxy-galaxy interactions and mergers is responsible for the unique morphology of such galaxies. This is supported indirectly by several pieces of evidence, including: the luminosity of the BCG is correlated with the cluster mass (Scott 1957; Lin & Mohr 2004) and X-ray luminosity (Hudson & Ebeling 1997); BCGs in the most X-ray luminous clusters are larger and have surface brightness profiles which are less steep than their low X-ray luminosity counterparts (Brough et al. 2005); and the velocity dispersion of BCGs rises less steeply with luminosity than for other bright galaxies (von der Linden et al. 2006). All this indirect evidence for a rich merger history is supported by high resolution imaging of BCGs obtained with the *Hubble Space Telescope*, which has revealed that the cores of these galaxies can be complex, often showing multiple nuclei and prominent dust signatures (Laine et al. 2003).

However, the evolutionary history of these galaxies is still not completely understood, and work on cooling flow (CF) clusters has hinted at another possible mechanism for adding to the stellar mass of BCG. The original cooling flow hypothesis is that hot cluster X-ray gas cools and condenses out of the intracluster medium (ICM) into the cluster's potential well, forming molecular clouds and stars (Fabian 1994). This drop-out occurs at the centre of the cooling flow, within the cooling radius, ie. onto the BCG. Cooling flow clusters are common in the local universe (making up about 50% of the population in an X-ray flux limited sample Peres et al. 1998; Chen et al. 2007)),

and cD galaxies are often found at the centre of these systems. Because of this, a link between the cooling X-ray gas and recent star formation in the BCG has been discussed for many years (Fabian 1994). Convincing observations which support this idea have been presented: a blue and UV-colour excess (McNamara et al. 1996, 2004; Hicks & Mushotzky 2005), molecular gas (Edge et al. 2002; Jaffe et al. 2001; Salomé & Combes 2003) and Hα emission (Crawford et al. 1999; Donahue et al. 2000; Crawford et al. 2005) have all been seen in the cooling flow cluster's BCG. However, although the morphology of the Hα emission is diffuse and filamentary, indicating star formation in some CF BCGs, in others it is very compact and more characteristic of AGN dominated emission (Donahue et al. 2000; Edwards & Robert 2007; Hatch 2007). As well, von der Linden et al. (2006) recently showed that optical emission lines in BCGs predominantly arise from LINER emission, rather than normal star formation.

More recent X-ray satellite measurements from *Chandra* and *XMM* have shown that the gas does not cool directly from the hot X-ray phase through to the cool molecular gas phase (Böhringer et al. 2002), but rather that a large amount of the cooling gas is being reheated before condensing out of the ICM. The current paradigm is that AGN activity in the BCG is reheating the cooling X-ray gas, which implies a more complicated feedback process between the cooling gas and the central galaxy (e.g Pizzolato & Soker 2005). This leads to revised, predicted mass deposition rates that are now in reasonable agreement with the observed values (Böhringer et al. 2002; Pizzolato & Soker 2005). The observed molecular and ionic gas may be attributed to a small amount that has cooled from the cooling flow; alternatively, the Hα may be excited by the AGN itself. Detailed studies of star formation indicators in galaxy groups and clusters in cooling flows and non-cooling flows, discriminating between those with and without AGN activity, are required in order to analyze the relative importance of the different processes.

A correlation between optical line emission in the BCG and cluster properties has been explored by several authors, most notably Crawford et al. (1999), who found that 27% of BCGs have optical line emission, and that the projected distance from the BCG to the X-ray centre is less for line emitting galaxies than for non-emitting galaxies. Recently, von der Linden et al. (2006) and Best et al. (2006) have explored the properties of BCGs in the SDSS, using the C4 cluster catalogue (Miller et al. 2005). These authors find that radio-loud AGN activity is more frequent in BCGs than in other galaxies of the same mass, but that this frequency does not depend strongly on cluster velocity dispersion. On the other hand, in their study of radio-loud properties of an X-ray selected cluster sample, Lin & Mohr (2006) find the overall radio-loud fraction to be 30% in BCGs, and that the fraction is higher in more massive clusters. Importantly, von der Linden et al. (2006) find that many of these radio-loud galaxies would not necessarily be identified as AGN from their optical emission lines and, in fact, that optical AGN activity appears to be *less* frequent among BCGs than other cluster galaxies of similar mass. The interpretation is complicated by the fact that the radio-selected galaxy sample, though restricted to red galaxies, could be contaminated by galaxies in which the low luminosity radio emission arises from star formation, rather than AGN activity.

In this paper, we explore optical line emission in BCGs with respect to properties of the galaxy and the host cluster, using two large, homogeneous datasets. One sample is taken from the X-ray selected, National Optical Astronomy Observatory Fundamental Plane Survey (NFPS), for which the X-ray properties are known for all clusters. For many of these clusters, we are able to identify those with short cooling times (CF clusters) based on *ROSAT*, *Chandra*, or *XMM-Newton* observations. We complement this sample with optically-selected clusters drawn from the Sloan Digital Sky Survey Data Release 3 (SDSS DR3), which is not biased toward X-ray luminous clusters, and is therefore more representative of the cluster population. In addition, the greater spectral coverage of the SDSS allows us to use emission line ratios to identify whether the emission arises predominantly from composite HII region and LINER activity, or from LINER activity alone (pure HII-region, and Seyfert-like emission are both rare).

The paper is organized as follows. In section 2, we introduce our galaxy samples and selection criteria. In section 3, we report our results. For the X-ray selected NFPS we compare the frequency of Hβ emission in BCGs as a function of BCG magnitude and distance to the cluster centre. Similar results are found for the SDSS sample, based on the Hα emission line. However, we find that there are differences between the BCGs in the two samples, which we can attribute to the nature of the X-ray emitting gas. In section 4, we consider the impact of our results on various galaxy and cluster formation hypotheses, and summarize our results. We conclude in section 5. Unless otherwise stated our analysis assumes the values $\Omega_{\rm m}$=0.3, for the matter density parameter, Ω_Λ=0.7 for the cosmological constant, and H_0=100 km/s/Mpc for the Hubble parameter. L_X refers to the bolometric X-ray luminosity throughout.

2 DATA AND SAMPLE SELECTION

For both NFPS and SDSS, our goal is to identify the BCG and a similar sample of luminous "control" galaxies that is located in the inner regions of the cluster. We first discuss the sample selection of the NFPS.

2.1 NOAO Fundamental Plane Survey

The NFPS is an all sky study of 93 X-ray selected rich clusters with redshifts between 0.010 and 0.067 (Smith et al. 2004). The goals of the project are to measure cosmic flows on the scales of 100 h^{-1} Mpc and to build a large homogeneous sample with which to investigate physical effects and environmental influences on early-type galaxy evolution and formation (Smith et al. 2004). The spectroscopic observations are made though a fiber diameter of 2" and are limited to red sequence galaxies; galaxies more than 0.2 magnitudes bluer than the red sequence were not generally observed spectroscopically. There are spectra for 5388 galaxies with a wavelength coverage between 4000 and 6100 Å and a resolution of $\sim$ 3 Å (Smith et al. 2004).

2.1.1 Cluster, BCG, and Control Sample Definitions

In order to respect the completeness of the NFPS cluster sample, we exclude the 13 clusters that were observed serendipitously and that did not meet the original L_X limit of $10^{42.6}$ erg/s. For each cluster, the redshifts were used to calculate the cluster velocity dispersion and the radius at which the mean density interior to the cluster is 200 times the critical density (σ_{cl} and r_{200}, respectively). We used the prescription $r_{200}=\sqrt{3}\sigma_{cl}/1000$ km/s/Mpc as derived in Carlberg et al. (1997). Note that r_{200} is typically of order 1.5 h^{-1} Mpc, much larger than the cooling radius of a typical cooling-flow cluster (about 200 kpc). The centre of the cluster is taken to be at the peak of the X-ray emission (Ebeling et al. 1996, 2000). The galaxies are then assigned to the clusters based on a radial and a velocity weighting as in Smith et al. (2004). For this analysis, we are interested in only the bright galaxies in the central regions of the cluster and so include a magnitude limit of $M_K < -24$, based on K-band total magnitudes obtained from 2MASS catalogues (Skrutskie et al. 2006). This is about half a magnitude brighter than the characteristic K-band magnitude of $M_{K*} = -23.55$ (Lin et al. 2004, for $H_0 = 100$ km/s/Mpc). Since we are interested only in galaxies occupying a similar environment as the BCG, ie. in the central regions of the cluster, we consider only galaxies within $0.5r_{200}$, and with velocity differences with respect to the cluster mean velocity less than twice the cluster velocity dispersion.

The BCG is then defined as the first rank cluster galaxy using the K-band magnitudes. In twenty cases, the BCG was not observed spectroscopically due to constraints in the fiber positioning, and these clusters have been excluded from our analysis. Our final sample consists of 60 clusters with BCGs, as summarized in Table 1 and listed in Table 2. Our control sample consists of the 159 other bright ($M_K < -24$) galaxies within the same radial and velocity cuts described above. The BCGs are, of course, excluded from the control sample.

For the NFPS, we use the stellar absorption-corrected Hβ emission as an indicator of star formation activity, since Hα is not generally available in these spectra. Although $H\beta$ emission is relatively weak, the high signal-to-noise ratio of these spectra allow us to measure its strength reliably after correcting for underlying stellar absorption (see the errors quoted in Table 2). The observed galaxy spectra are divided by best fit absorption template stellar population synthesis models from Vazdekis (1999), which have been redshifted and broadened to match the velocity dispersion of the observed galaxy. Subsequently, the Hβ equivalent width is measured directly, without assuming a particular line profile, from the ratio of the observed spectrum to the best fit model (Nelan et al. 2005). A thorough discussion of the emission line measurements can be found in Nelan et al. (2005). For two of the NFPS BCGs, in Abell 780 and in Abell 1795, the nebular emission is strong enough that our standard methods for obtaining reliable velocity dispersions, and hence stellar absorption corrections, fail. For galaxies of similar magnitude, the typical stellar absorption at Hβ is $\sim$1.5 Å with an uncertainty of 0.3 Å. This error dominates our uncertainity in the total equivalent width of emission for these two special cases. For the BCGs in Abell 780 and Abell 1795, the Hβ equivalent widths are 7.8 Å and 7.2 Å, respectively. However, to achieve a plot that is more easily read, these points are set to respective lower limits of 3.3 Å and 3.7 Å in Fig. 5 and Fig. 6.

We will define emission-line galaxies to be those with an equivalent width > 0.5 Å. Since the Hα and [NII] lines are generally unavailable, we are unable to use Baldwin et al. (1981, hereafter BPT) diagrams to reliably distinguish emission due to star formation from that arising from AGN activity.

2.1.2 Cooling Flow definition

In general, we designate an NFPS cluster as "cooling flow" (CF) or "non-cooling flow" using mass deposition rates and X-ray cooling times from published catalogues (Peres et al. 1998; White 2000; Allen et al. 2001; Bîrzan et al. 2004). This is a somewhat subjective classification complicated by the fact that not only are mass deposition rates calculated from *ROSAT* observations typically 2-10 times higher than those calculated from *Chandra* observations (Böhringer et al. 2002), but also higher resolution spectra from *XMM Newton* are not well matched to an isobaric cooling model (Peterson et al. 2003); thus the mass deposition rate may not be an exact indicator of a cooling flow cluster. Therefore, whenever possible, we prefer to use recent cooling flow designations based on the presence of a central temperature gradient in *XMM Newton* or *Chandra* observations. For the rest, we are left with using the mass deposition rate based on *ROSAT* data as an indicator. For the 11 cases where observations are from the *Chandra* or *XMM Newton* satellites, we define a CF cluster to be one with a mass deposition rate $\dot{M} > 0$; otherwise, we require $\dot{M} > 100 M_{\odot}\mathrm{yr}^{-1}$. Within this framework we have 14 CF clusters and 19 non-CF clusters. The CF status of another 27 clusters is unknown. Clearly this is not an unassailable definition; however, it is likely that most, if not all, of the clusters we classify as CF clusters really do have short cooling times in the centre. Some galaxies with low mass deposition rates will undoubtedly fall in our non-CF sample. With this in mind, our results are not sensitive to this definition. We further discuss this point in Section 3.1, as well as a continuous method of defining a CF cluster, based on an excess of observed X-ray luminosity to predicted values (McCarthy et al. 2004).

2.2 Data from the Sloan Digital Sky Survey

Our second sample of galaxy clusters is derived from the C4 catalogue (Miller et al. 2005), based on the third data release (DR3) of the SDSS. This release covers 5282 square degrees in imaging, and 4188 square degrees in spectroscopy (Abazajian et al. 2005). Imaging was taken in five optical bands, u', g', r', i' and z' with a median spatial resolution of 1.4" in r'. Spectra are observed with a aperture diameter of 3", cover the wavelength range from 3800 to 9200 Å and have a spectral resolution of $\sim$3 Å in r'. Redshifts measured from these spectra are accurate to $\sim$ 30 km/s (Abazajian et al. 2005). The Hα line strengths are measured by fitting gaussians to the line profile in a standard pipeline (Stoughton et al. 2002). For $W_\circ(H\alpha) > 5$Å, the equivalent width uncertainty is less than 20%. For weaker lines, $W_\circ(H\alpha) < 5$Å the errors are known to be large

(Gómez et al. 2003). We have made no correction to the emission-line strengths for underlying stellar absorption. For our purposes this is safe to neglect because, whereas even a modest star formation rate generates considerable Hα emission, the stellar absorption doesn't vary by more than ~ 1 Å for moderately old populations.

As described in Miller et al. (2005), clusters and groups are identified as overdensities in the multi-dimensional space spanned by position, redshift, and five-colour photometry. There are 1106 clusters identified in the SDSS DR3 using this algorithm. We further select objects with redshifts $z < 0.10$, to minimize the incompleteness of the sample. In order to reduce the number of clusters with uncertain velocity dispersions, we exclude clusters flagged as having significant substructure. Specifically we include only clusters flagged as SUB=0, ie. those for which the ratio of the standard deviation of the cluster velocity dispersion profile to the mean cluster velocity dispersion is less than 15 (Miller et al. 2005). This reduces the number of clusters in our sample to 825.

2.2.1 Cluster, BCG, and Control Definitions

For the SDSS we define the BCG and clusters in as close a manner as possible to the NFPS case. Again, the BCG is the brightest galaxy in the K band (and with $M_K < -24$), within half of r_{200} of the geometric centre of the cluster, and within two times the cluster velocity dispersion. However, the geometric centres we use are different than those in the C4 catalogue. We start with the C4 catalogue geometric centres measured using the luminosity weighted position average of all the galaxies within 1Mpc and four times the velocity dispersion. As this definition encompasses such a large area, multiple substructures along the line of sight heavily influence the position of the centre. For example, the geometric centre will be placed in between two obvious subclumps. Thus, we iteratively recalculate a luminosity-weighted centre using only galaxies within two times the cluster velocity dispersion, and with magnitude $M_K < -24$.

Due to the incomplete spectral coverage of the central galaxies, there are 154 cases in which the brightest cluster galaxy had not been observed spectroscopically. We exclude these clusters from the sample. To ensure this is not introducing an important bias, we verified that the subset of BCGs observed in the photometric catalogue but not in the spectroscopic catalogue have an equivalent $(u' - r')$ colour distribution to those in our final, spectroscopic sample. Finally, we also remove those clusters whose geometric centres are within 15' of a survey boundary, as well as those with measured velocity dispersions greater than 1200 km/s. The latter restriction is made because such high values are usually a result of significant contamination from line-of-sight substructure. These selections leave us with a final sample of 328 BCGs.

Our control sample is built from the other bright galaxies near the centre of the clusters, as in the NFPS case. In order to increase the size of our control sample, we include clusters where the brightest central galaxy was not measured spectroscopically. There are 526 control galaxies in 353 groups and clusters with a velocity dispersion less than 1200km/s. We note that the number of control galaxies per cluster is significantly larger in the X-ray luminosity selected NFPS clusters, probably because they are richer than the optically-selected SDSS clusters.

Because the centres of the NFPS clusters are based on the X-ray centroid, whereas in the SDSS the geometric centre is used, it is important to compare the two definitions. In order to find X-ray centers for the SDSS clusters, we have matched them to X-ray cluster catalogues including: NORAS (Böhringer et al. 2000), REFLEX (Böhringer et al. 2001), BAX (Sadat et al. 2004), XBACS (Ebeling et al. 1996), RASSCALS (Mahdavi et al. 2000), as well as Popesso et al. (2004); Mulchaey & Zabludoff (1998) and Horner et al. (2001). Most of the cluster catalogues are based on *ROSAT* observations, where the flux limit is high. This restricts our sample of SDSS clusters with X-ray detections to the small subset of massive clusters at $z < 0.03$. There are 35 X-ray cluster matches, ie. cases where the X-ray centre is within half of r_{200} of one of our 328 SDSS clusters. Fig. 1 shows that for most of the matched clusters, there is good agreement between the X-ray and geometric centres. However, also depicted in the figure is how some cases exhibit differences of up to 0.5 Mpc, especially for lower mass clusters. It is unlikely that this is caused by an uncertainty in the X-ray centres, as the centres of the NORAS, BCS, and XBACS samples were found by determining the two-dimensional centre of mass using the Voronoi Tessellation and Percolation method (Ebeling & Wiedenmann 1993), and are generally accurate to about 1' (Ebeling et al. 1998), corresponding to ~ 90 kpc at $z \sim 0.08$. More likely, is that the geometric centers do not trace the gravitation potential of the cluster as well as the X-ray centres. We note that for many of the cases in which the centres are discrepant by > 200 kpc, the geometric centre appears to be contaminated by in-falling groups; which is not surprising as it is measured using a typical line of sight projection of ~ 3 Mpc (for $\sigma = 500$km/s).

2.2.2 Emission Line diagnostics

Optical emission line galaxies in the SDSS are identified from the Hα line, which is the line in our wavelength range that is most sensitive to star formation activity. To ensure a fair comparison with the NFPS, we must choose a threshold in Hα equivalent width that is comparable to the Hβ limit used in that survey. Recall that the lines are measured using different techniques, from spectra of different resolution and signal-to-noise, and obtained with different fibres; furthermore, the NFPS Hβ measurements are corrected for underlying stellar absorption, while the SDSS Hα lines are not. Therefore we opt for an empirical "calibration" between the two, by plotting the NFPS Hβ equivalent widths against the SDSS Hα equivalent widths, for galaxies that appear in both surveys (Fig. 2). Although there is plenty of scatter, there is a strong correlation between the two lines, and we find the Hα index is about four times larger than the Hβ; encouragingly, this is comparable to the factor of 4.5 derived by comparing the Hα/Hβ ratio for the subset galaxies in the NFPS for which measurements of both emission lines are available (Nelan et al. 2005). Thus, an Hα equivalent width cut of 2 Å is comparable to an Hβ equivalent width of 0.5 Å, and the fraction of galaxies in our samples above either of these thresholds is similar. Note that the points at $W_\circ(H\alpha) = 0$ are non-detections (plotted with the aver-

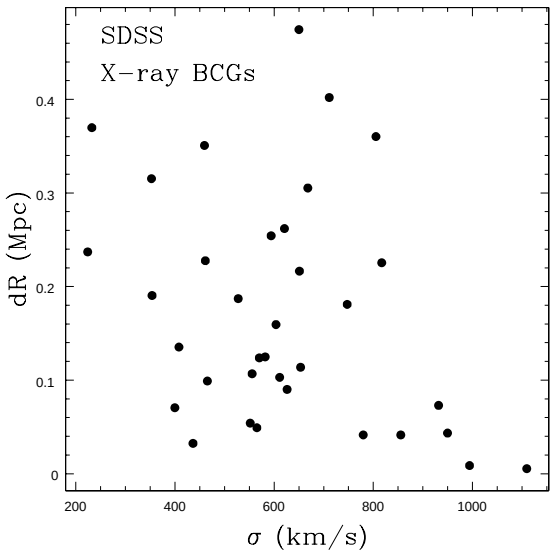

Figure 1. Cluster velocity dispersion as a function of the difference in the X-ray and geometric centres for the 35 SDSS BCGs that have available X-ray positions. The clusters with large discrepancies between the two centres are generally found to have geometric centres highly influenced by in-falling groups.

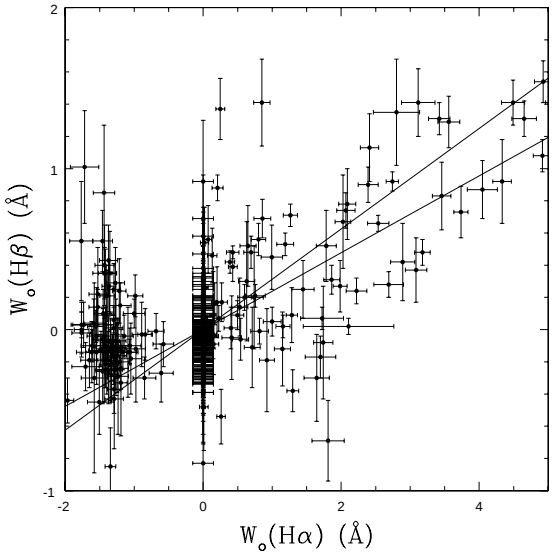

Figure 2. The absorption-corrected NFPS Hβ equivalent width versus the SDSS Hα equivalent width (uncorrected for absorption) for galaxies present in both surveys. The points with $W_o(H\alpha) = 0$ are non-detections (plotted with the average Hα error of 0.15Å), and those with $W_o(H\alpha) < 0$ are detected in absorption. We identify line-emitting NFPS galaxies as those with W_o (Hβ) $\geq$ 0.5 Å. Correspondingly, we use a value of W_o (Hα) $\geq$ 2 Å for the SDSS galaxies. The best fit lines are constrained to go through (0,0) and are only fit to galaxies with W_o (Hα) $\geq$ 2 Å and ignore an outlier at W_o (Hα) $\approx$ 40. The two different lines are fitting for W_o (Hβ) as a function of W_o (Hα) or vice versa.

age uncertainty of 0.15Å), and those with $W_\circ(H\alpha < 0)$ are detected in absorption. We have experimented with SDSS Hα equivalent width cuts of 2$\pm$1 Å and find that our final results do not change significantly. The good correlation also gives us additional confidence in the template correction used to correct the Hβ equivalent widths for stellar absorption, which is relatively much more important here than for Hα (the average stellar absorption strength is $\sim$ 1 Å, with variations at the $\sim$ 0.15 Å level).

Due to the proximity of the galaxies in our sample and the finite fiber size though which they are observed, the amount of extended line emission could be underestimated. However, as we do not know if the emission is extended we have not explicitly accounted for the finite fiber size, nor for the difference in fiber diameters between two surveys. Here again, we argue that the effect on the line strength measurements is calibrated by our use of an empirical relation.

Hα line emission may arise from either ionization by hot stars, or ionization from AGN activity. We use the AGN classification taken from the emission-line analysis discussed in Kauffmann et al. (2003), which is based on Hα/[NII] and [OIII]/Hβ diagnostic ratios, which separates AGN, star-forming, and composite (intermediate between star-forming and AGN) regions on BPT diagrams. Table 1 shows that, in our SDSS sample, $\sim$ 65 % of galaxies with emission have line ratios consistent with AGN or composite emission, and this fraction may be somewhat higher for the BCG population, relative to the control galaxies. Using Ho et al. (1997) to separate Seyferts from LINERs, along with the Kauffmann et al. (2003) definitions, we find that $\sim$ 33% of emitting SDSS BCGs can be reliably measured as LINERs, $\sim$ 27% as composite; Seyfert-like emission is negligible ($\sim$ 3%). If we assume the ionizing source for the HII regions is stellar, and that all of the Hα emission is within the fibre diameter, then typical Hα luminosities of our emitting BCGs correspond to star formation rates of ~ 0.5 to $\sim 1.6\ M_\odot \mathrm{yr}^{-1}$ (Kennicutt 1998).

2.2.3 Galaxy Colour

Fig. 3 shows the distribution of Hα equivalent width as a function of $(u' - r')$ colour. Following Strateva & Knapp (2001), we use the value of 2.2 for the $(u' - r')$ colour separation of blue and red galaxies. As the NFPS galaxies are red selected, we include a corresponding colour cut of $(u' - r') > 2.2$ for the SDSS galaxies when directly comparing to the NFPS results (as in Section 3). This colour cut excludes 10 of the 328 SDSS BCGs (only one with X-ray data) as well as 53 control galaxies.

As seen in Fig. 3, most BCGs are redder than this cut whether or not they show optical emission. Thus, if the line emission is due to star formation, it does not dominate the global colours of these BCGs, which are presumably quite old. Because of this, results based on BCGs in the NFPS are not likely to be affected by the colour cut in that sample. For the control sample, most of the emission-line galaxies are bluer than our cut. Therefore we expect the fraction of control galaxies with emission, as presented in Section 3, to be biased low relative to the BCGs. This is evident from Table 1: in the red-selected SDSS sample, the overall fraction of emission line galaxies is similar ($\sim$ 11 %) for both control galaxies and BCGs, while for the unrestricted sample the fraction of control galaxies with emission is $\sim$ 18%. This

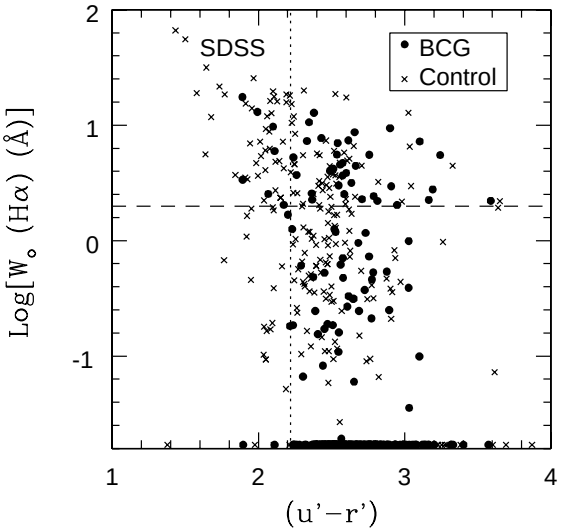

Figure 3. The logarithm of W$_o$ (Hα) as a function of $(u' - r')$ colour of the galaxies in the SDSS. The crosses are the control sample, and the filled circles are the BCGs. The colour break of 2.2 is shown as the vertical dotted line, and the horizontal dashed line separates the emitting galaxies from the quiescent. The galaxies at Log[W$_o$ (Hα)] = -1.7 are those with Hα absorption.

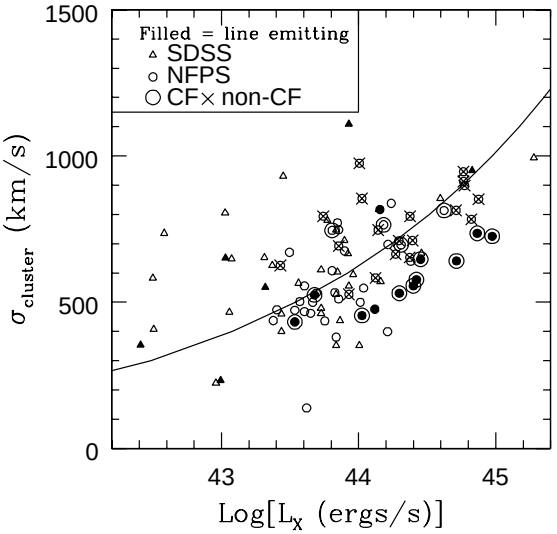

Figure 4. The cluster velocity dispersion as a function of the bolometric X-ray luminosity. The solid line is the preheated model from Babul et al. (2002), which is known to provide a good match to non-CF clusters (McCarthy et al. 2004; Balogh et al. 2006). Known CF clusters in our sample do generally lie to the right of this model.

difference is not large enough to affect any of our conclusions in Section 3, however.

3 RESULTS

In this section we examine the line emission in the galaxies in our cluster samples as a function of X-ray luminosity, K-band magnitude, and distance from the centre of the cluster. The numbers of emission-line galaxies in both surveys are given in column 4 of Table 1. There is a higher fraction of emitting galaxies among the NFPS BCGs; 20±6% are emitting, compared to only 9±2% of the controls. If we look only at those BCGs identified with a CF cluster we find an even higher fraction of them show emission, 71^{+9}_{-14}, while the control sample is unchanged (14±6%). On the other hand, only 11±2% of the red BCGs selected from the SDSS sample show emission, comparable to that of the control population (11±2%). In this section we will explore these trends, and differences between the two samples, in more detail. We use errors derived from the posterior probability distribution where sample sizes are small.

3.1 Dependence on the Presence of a Cooling Flow

The most prominent result from the NFPS clusters is that the presence of a cooling flow is highly correlated with the presence of emission lines in the BCG. Fig. 4 shows the bolometric X-ray luminosity against the cluster velocity dispersion (a proxy for dynamical mass). We can see that most of the cooling flow clusters have larger X-ray luminosities for their mass, and that it is these clusters that have a BCG with line emission. Therefore, in the rest of the NFPS analysis we separate our sample into CF and non-CF subsets. Notice that in Fig. 5 and Fig. 6 (which we discuss below), none of the emitting BCGs are non-CFs. As mentioned in Section 2.1.1, we use a rather strict cut for our definition of a CF, requiring *ROSAT* based $\dot{M} > 100 M_{\odot} yr^{-1}$. However, changing our arbitrary definition of a CF cluster (e.g. to those with $\dot{M} > 10 M_{\odot} \mathrm{yr}^{-1}$) does not significantly change our results.

It would be useful to have a way to identify likely cooling-flow clusters without the need for high quality surface brightness and temperature maps. Recently, McCarthy et al. (2004) has shown that CF clusters show significantly higher total X-ray luminosities, relative to their total dynamical mass, consistent with predictions from steady-state cooling models. On the other hand, non-CF clusters can be well modelled with cosmological haloes in which the gas has been preheated to $\sim 300 - 500$ keV cm^2 (Balogh et al. 2006, see also). This suggests that one could use the excess X-ray luminosity relative to these preheated models as an indicator of CF status. The solid line in Fig. 4 represents models for clusters with preheating from Babul et al. (2002). Indeed, using this method arrives at results for the emission fraction which are very similar to those obtained when we use the mass deposition rate to define CF clusters. The separation is not as striking as in McCarthy et al. (2004), probably because the measured velocity dispersion can be systematically affected by substructures.

3.2 Magnitude Dependence

We show in Fig. 5 the line emission strength as a function of K absolute magnitude for the NFPS and SDSS BCGs and

Table 1. Summary of Results. The first column presents the survey studied, NFPS or SDSS. SDSS (RED) includes only the red-selected SDSS galaxies, and SDSS (X-ray) only those with X-ray counterparts. Column 2 indicates if the results are for the BCGs or Controls. Column 3 shows the total number of galaxies for each sample. The number of these which are emitting is shown in column 4, and column 5 shows the fraction of emitting galaxies. Column 6 lists the number of strongly emitting ($W_o(H\alpha)> 2$Å) galaxies in each sample for which the emission line ratios are characteristic of AGN activity (usually LINER). We present the number of galaxies in our sample which are known to belong to a CF cluster in column 7. Column 8 shows the number of these galaxies in CF which are also emitting, and the final column shows the fraction of emitting galaxies in CF clusters.

Survey	Sample	Total	Emitting	Emitting Fraction(%)	AGN or Comp. $W_o(H\alpha)> 2$Å	Known CF	Emitting CF	Emitting Fraction(%)
NFPS	BCGs	60	12	20±6	N/A	14	10	71^{+9}_{-14}
	Controls	159	15	9±2	N/A	36	5	14±6
SDSS	BCGs	328	42	13±2	31	N/A	N/A	N/A
	Controls	526	94	18±2	57	N/A	N/A	N/A
SDSS (RED)	BCGs	318	35	11±2	25	N/A	N/A	N/A
	Controls	446	51	11±2	39	N/A	N/A	N/A
SDSS (X-ray)	BCGs	34	6	18^{+8}_{-5}	3	N/A	N/A	N/A

control galaxies. The NFPS clusters are separated into CF and non-CF cases. In the non-CF clusters, there are no emitting BCGs, and the fraction of emission-line galaxies, shown in the bottom panels, is also very low for the control galaxies (~ 5 %). On the other hand, in CF clusters ~ 70 % of the BCGs show emission, as we noticed also in the previous section. Moreover, the BCGs with strong emission tend to be the brightest galaxies, $M_K < -25.5$, where by definition, there are few control galaxies. Hence, this trend is quite different from what is seen in the control sample, where almost all of the emission line galaxies are fainter than $M_K = -25$. For magnitudes near $M_K \approx -25$, where there is substantial overlap between the two populations, the emission line fraction of both populations are similar for non-CF clusters. The results from the SDSS, which include all clusters regardless of X-ray luminosity or CF status, are consistent with the results for the total NFPS. There are somewhat fewer emission-line BCGs at a given magnitude than the for NFPS, presumably because CF clusters make up a smaller proportion of the sample in the SDSS. We will say more about this in Section 4.

Also highlighted on Fig. 5 and Fig. 6 are the BCGs with LINER-like emission. Most of the emitting BCGs are more characteristic of LINER emission; this is especially true of the less luminous BCGs.

3.3 Dependence on Location in Cluster

In our samples, there are some BCGs that are found close to the X-ray centre, while others can be found several hundred kpc away. In this section we will investigate whether or not the presence of emission lines in the BCG depends on its distance to the X-ray centre.

This is illustrated in Fig. 6 where we show the line emission as a function of cluster radius for the NFPS galaxies. *All of the strongly emitting BCGs are within 50 kpc of the X-ray centre.* As discussed in the previous section, these emitting galaxies are also usually found in a cooling flow cluster. In the rightmost panel we show the equivalent plot for the 34 BCGs in the SDSS sample for which we have X-ray centres. Although the sample is small, our results are consistent with those seen in the NFPS; only those BCGs that are close to the X-ray centre have significant line emission.

A Kolmogorov-Smirnov test on the Hβ distributions of the non-CF BCGs and the controls shows no evidence for a difference in the two populations. Therefore, to summarize, we conclude that an increased frequency of optical line emission in BCGs is observed only for those galaxies that lie within 50kpc of the X-ray centre of a CF cluster. For the remainder, the frequency of emission in BCGs is consistent with that observed in the control population.

3.4 Dependence on Cluster Mass and Density

The SDSS provides us with an optically-selected sample, spanning a wide range in velocity dispersion, that should be representative of the cluster population independent of X-ray properties. In this section we use this full sample (including those galaxies with $(u' - r') < 2.2$ that were excluded when comparing directly with the NFPS) to explore the effect of environment on the presence of line emission in BCGs.

Since the cooling flow status of a cluster might be correlated with its total mass, or central mass density, we wish to explore whether the trends we have observed are merely reflecting a more fundamental correlation with either of these quantities. First, in Fig. 7, we plot the fraction of BCGs with Hα emission as a function of the cluster velocity dispersion. There is no strong trend. Rather, a fraction $\sim$ 10-15 % of BCGs in each bin showing Hα emission is observed (the Spearman correlation coefficient is 0.17). We note that the frequency of radio-loud AGN is also found to be independent of velocity dispersion (Best et al. 2006). The control galaxy population in the SDSS sample also shows no strong correlation between emission line fraction and group velocity dispersion (the Spearman correlation coefficient is 0.38). For the control galaxies, the overall fraction of emitting galaxies is somewhat higher than for BCGs, closer to 15-20%.

Next, we examine in Fig. 7 the frequency of emission lines in BCGs as a function of the galaxy density, as measured by the distance to the fifth-nearest spectroscopic neighbour. Even in the densest regions this corresponds to a smoothing scale of ~ 200 kpc, so the measurement here is of the total mass density on scales larger than the cooling radius. Generally, one would expect the central regions of CF clusters to be the densest environments, and if the pres-

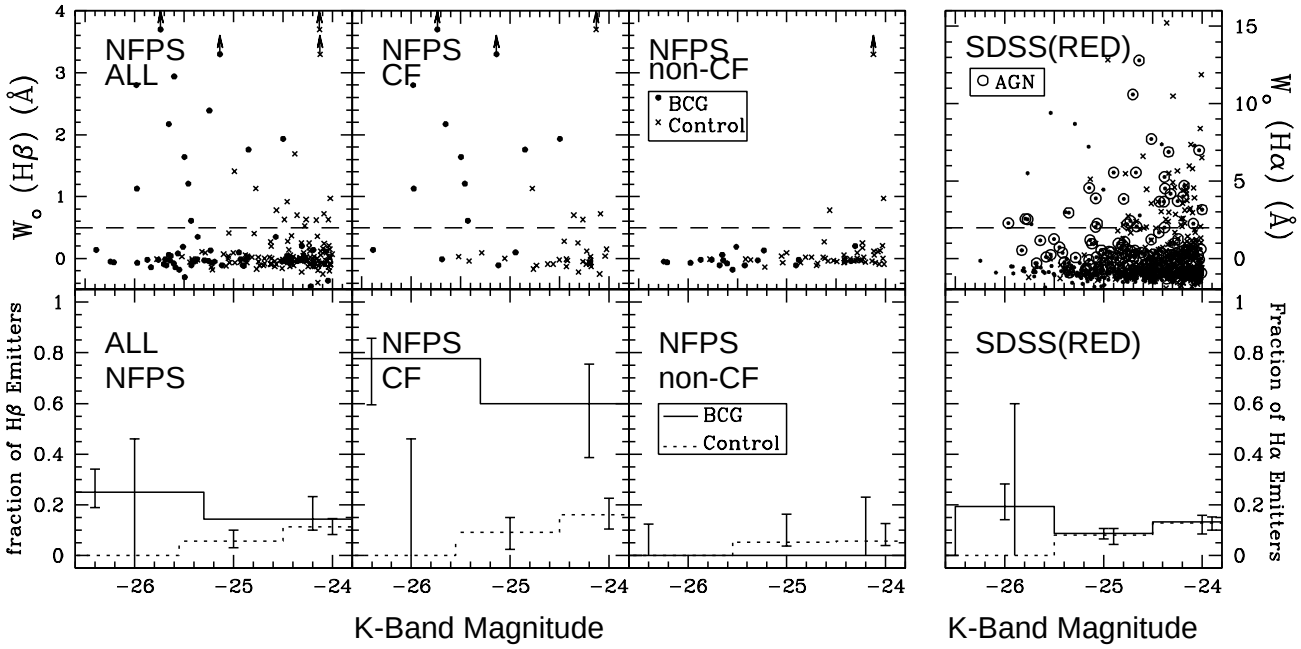

Figure 5. Line Emission as a function of K-Band Magnitude. Top Panel: The equivalent width of the line emission as a function of K-band magnitude for the NFPS galaxies on the left, and for the SDSS galaxies on the right. The NFPS galaxies are in subsets: a) All galaxies, including those in clusters where the CF status is unknown, b) those which are in known CF clusters, and c) those which are in known non-CF clusters. Filled circles represent BCGs, Xs for control galaxies, and open circles indicate LINER emission (for the SDSS sample only). The dashed line represents the cut between emitting and non-emitting galaxies. The BCGs for Abell 780 and Abell 1795 have unreliable Hβ equivalent widths, but nonetheless strong emission, and are represented by lower limits at $W_o > 3.3$ Å and > 3.7 Å, respectively. Bottom Panel: Using the same subsamples as the top panel, we plot the fraction of line emitting galaxies as a function of K-band magnitude. The solid line represents the BCGs, and the dotted line the control galaxies.

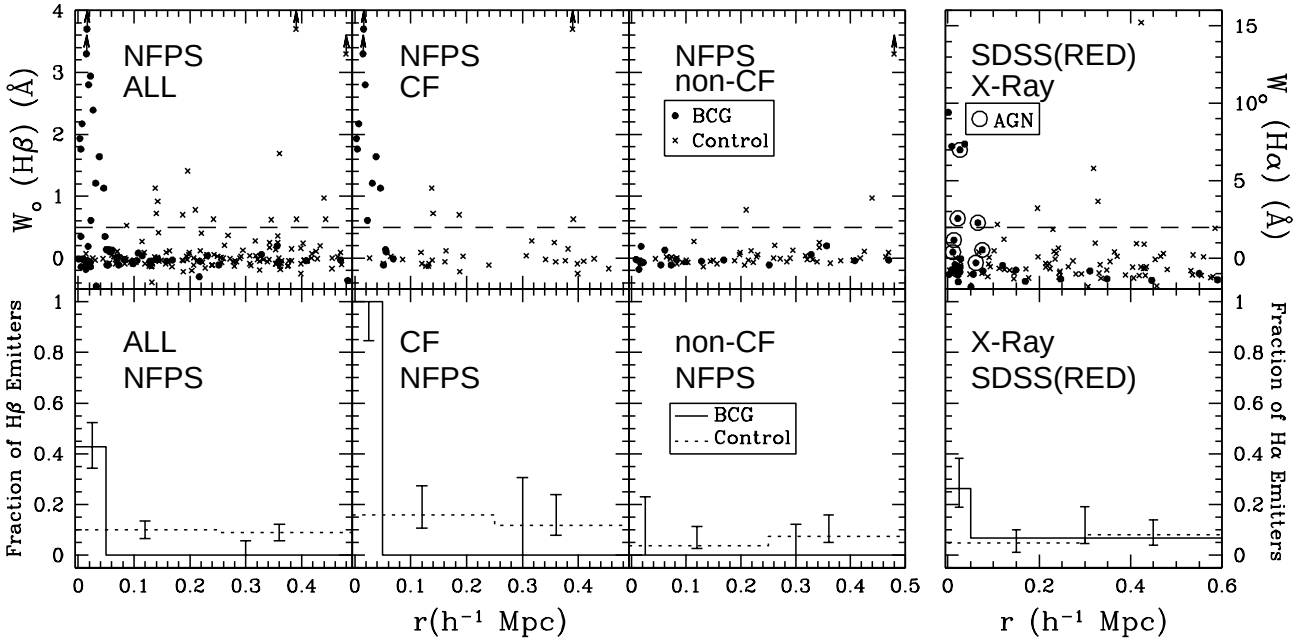

Figure 6. Line Emission as a function of distance from the cluster X-ray centre. Subsample definitions and symbols are the same as in Fig. 5.

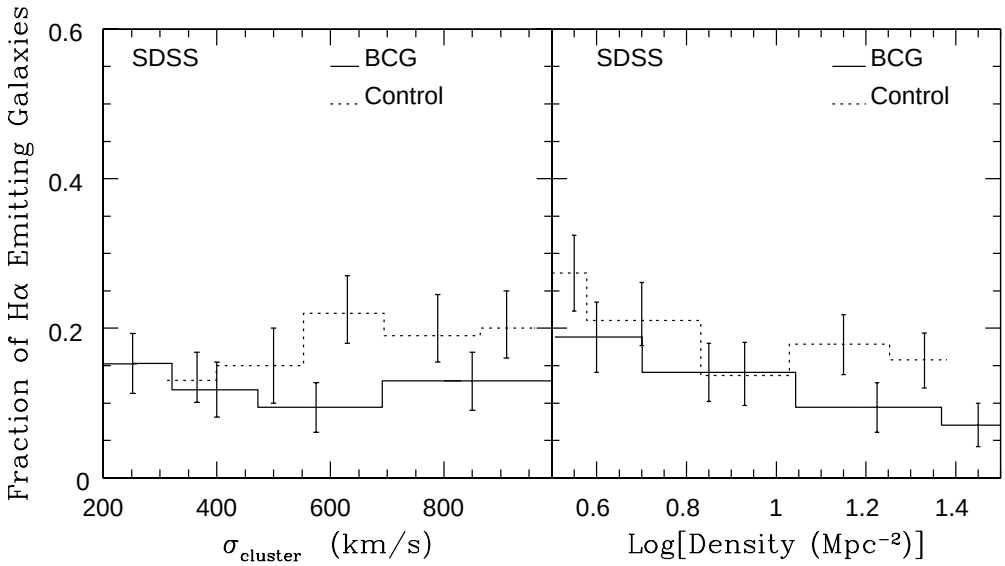

Figure 7. Left Panel: The fraction of Hα emitting galaxies in the SDSS as a function of group velocity dispersion. The solid line refers to BCGs and the dotted line are the control galaxies. This adaptive histogram contains 85 galaxies per bin for the BCGs and 100 galaxies per bin for the controls. Right Panel: The fraction of Hα emitting galaxies in the SDSS as a function of the galaxy density. This adaptive histogram contains 85 galaxies per bin for the BCGs and 95 galaxies per bin for the controls.

ence of a cooling-flow was correlated with the mass or galaxy density on larger scales our previous results would lead us to expect the most star formation occurring in the most dense regions. On the contrary, we observe a clear correlation with the emission line fraction decreasing with increasing number density, and so BCGs are *less* likely to show emission lines if they are found in the densest regions of clusters (in both cases of the BCG and the controls, the Spearman test yields a correlation coefficient of ~ 0.9, and the correlation is significant at the $\sim 95\%$ confidence level). At all densities, the fraction of emission-line galaxies is higher in the control population than the BCG population. The fact that we observe enhanced emission for those galaxies within the smaller 50 kpc scale of the X-ray centre of CF clusters (Section 3.3) is therefore very likely related directly to the presence of cooling, X-ray gas on small scales, rather than the overall gravitational potential.

4 DISCUSSION

The overall fraction of BCGs with emission lines is ~ 13 % in the SDSS, and ~ 20 % in the NFPS. The latter is in good agreement with Crawford et al. (1999) who find a fraction of 27 % emission-line BCGs in their sample of X-ray selected clusters. We do not know what the CF fraction is in an optically-selected sample, or as a function of mass. Nonetheless, since the fraction of massive clusters that host a cooling flow is likely no more than about 50 % (Peres et al. 1998; McCarthy et al. 2004; Chen et al. 2007), and CF clusters are systematically overluminous, we attribute the factor of two difference in emission fraction between our two surveys to the fact that NFPS (and Crawford et al. 1999) is X-ray selected, and therefore biased toward CF clusters.

There is currently much observational and theoretical work exploring the possible feedback between a central galaxy's AGN, current star formation, and the cooling X-ray gas (Silk & Rees 1998; Best et al. 2006; Croton et al. 2006; Bower et al. 2006; Sijacki & Springel 2006; De Lucia & Blaizot 2006, e.g.). AGN in the BCGs are thought to play an important role in suppressing cooling, and lowering mass deposition rates (and hence star formation rates). Our main result is that the majority of line emitting BCGs are positioned close to the X-ray centre of clusters classified as hosting a cooling flow directly from the mass deposition rates (as defined in Section 2.1.1). Furthermore, this result holds when we classify cooling flow clusters instead by their excess X-ray luminosity relative to other clusters with similar dynamical mass (a definition we explored at the end of Section 3.1). Similar conclusions, based on smaller samples, have been reached by others (e.g. Johnstone et al. 1987; McNamara & O'Connell 1989; Crawford et al. 1999; Rafferty et al. 2006). Importantly, we have shown that, in the absence of a cooling flow, emission lines are rare in BCGs, regardless of the mass density or velocity dispersion of the cluster. Moreover, a control population of similarly bright, centrally located cluster galaxies does not exhibit an increased frequency of emission lines in CF clusters. We therefore conclude that the observed emission (arising from star formation and/or an AGN) is directly related to the presence of cooling gas.

For the most part, we have not concerned ourselves with the origin of the observed emission, since starburst galaxies and optically-selected AGNs are probably closely linked (Kauffmann et al. 2003). However, it is worth investigating this further here. Crawford et al. (1999) find that the very strongest Hα emitters have star formation-like emission line ratios, while von der Linden et al. (2006) find that most BCGs, which display weaker Hα emission, are more characteristic of LINER activity. The six NFPS BCGs that have [NII]/Hα line ratios available from Crawford et al. (1999) lie in the regime straddling LINERS and Seyferts. Of the

six emitting BCGs in the SDSS-X-Ray sample, the three stronger Hα emitters are non-AGN, which means that they are likely composite, whereas the somewhat weaker emitters are classified as AGN. Thus the emission-line BCGS found near the X-ray centre of galaxy clusters appear to be a heterogeneous class of objects.

In the unrestricted SDSS sample, we find only ~ 13 % of BCGs have line emission, compared to ~ 18 % for controls. This exhibits the same trend as in the von der Linden et al. (2006) study of SDSS C4 cluster galaxies, where detectable emission line luminosity measurements (with S/N >3) are found in 30 % of BCGs, as opposed to 40 % for the other massive, central, galaxies (ie. controls). Our numbers cannot be compared directly, as their cut includes more weakly emitting systems as emitters than does our more strict criterion of $W_o > 2$ Å. If we relax our definition of an emitting galaxy being one with $W_o > 0$ Å, we find the percentage of line emitters increases to 27 % for BCGs, and 38 % for controls.

Our Fig. 7 reiterates the above point, that in the SDSS sample, the BCGs have a lower fraction of line emitting galaxies than the controls. This is also consistent with what Best et al. (2006) find: that emission line AGN activity is suppressed in the galaxies near the centre of the cluster with respect to the other massive cluster galaxies. They point out that emission line AGN and radio-loud AGN are partly independent populations, but that BCGs with emission-line AGN are more likely to host radio-loud AGN than other galaxies. Best et al. also find that radio-loud AGN are preferentially found in BCGs within 0.2 r_{200} of the centre of the cluster and that there is a strong dependence on galaxy stellar mass, with ~ 40 % of the most massive galaxies showing radio loud AGN emission. Therefore it is plausible that our emission-line BCGs in the NFPS (which are found at the centre of CF clusters) and in the SDSS (many of which show LINER-like activity), host radio-loud AGN. We therefore matched our NFPS BCGs to radio sources from the Faint Images of the Radio Sky at Twenty-Centimeters survey (White et al. 1997, hereafter FIRST) and NRAO VLA Sky Survey (Condon et al. 1998, hereafter NVSS). We find that indeed, all 12 of our Hβ emitting BCGs are radio sources. Furthermore, for the 50 BCGs in the FOV of the surveys, 28 of our BCGs have radio counterparts ($\sim 56\pm11$ %). Thus $\sim 42\pm11$ % of non-Hβ emitting BCGs have radio emission. Again, the cooling flow status of the cluster appears important: $\sim 71^{+\ 9}_{-14}$ % of CF BCGs are radio sources, and $\sim 80^{+\ 7}_{-16}$ % of central CF BCGs are radio sources. For non-CF BCGs only $\sim 32^{+12}_{-\ 9}$ % have radio emission. For the controls, 36 of 144 galaxies in the FOV of the surveys are radio sources ($\sim 25\pm4$ %).

Recently, Lin & Mohr (2006) have studied the radio-loud properties of a large X-ray selected cluster sample, and find the overall radio-loud fraction to be ~ 35 % for K-band selected BCGs within r_{200} of the cluster center (compared with ~ 20 % for bright cluster galaxies, excluding the BCGs). This is in reasonable agreement with our results, although the radio-loud BCG fraction we measure is somewhat higher. Lin & Mohr (2006) also find a strong trend with cluster mass (inferred from the X-ray luminosity), though the strength of the trend is sensitive to the radio power limit and K-band luminosity of the galaxy. Our NFPS sample is too small to robustly identify such trends, but we note that the fraction of BCGs with radio sources that are in clusters with a velocity dispersion < 600km/s is 54±15 %, quite similar to that for BCGs in clusters with a velocity dispersion > 600km/s, 58±15 %. In the optically-selected SDSS, we find no significant trend with velocity dispersion, but an overall fraction of ~ 40 % of the BCGs with radio emission, and ~ 25 % of the controls. Because of the difference in sample selection, and the cluster mass estimators, we do not consider this a serious discrepancy with the results of Lin & Mohr (2006).

5 CONCLUSIONS

We have used two large, homogeneous galaxy cluster surveys to investigate the incidence of optical emission lines amongst BCGs. The NFPS consists of 60 BCGs in X-ray selected clusters, while the SDSS sample is a larger, optically-selected sample of 328 BCGs. From these data, we are able to draw the following conclusions:

- Of the 10 BCGs that lie within 50kpc of the peak of X-ray emission in a cluster with evidence for a significant cooling flow, all show optical emission lines. Moreover, of the 12 BCGs that show emission, all are located within 50kpc of the X-ray emission peak, all are radio sources, and none are in clusters of known non-CF status (10 are in CF clusters, and 2 are in clusters with unknown CF status).
- Excluding the special circumstances noted above, the fraction of BCGs that exhibit optical emission lines is $\sim$ 10-20 %, and is always comparable to or lower than the fraction for control galaxies with a similar luminosity and environment.
- For optically selected cluster samples, which are dominated by non-CF clusters, the fraction of BCGs with emission does not correlate strongly with cluster mass or galaxy density.

We have therefore demonstrated a direct connection between the presence of cooling gas, and enhanced optical emission in a centrally located galaxy. It would be very useful to obtain pointed X-ray observations of those SDSS clusters in which we have found a BCG with Hα emission, to determine if this correlation holds in optically-selected samples. These clusters would also be potentially interesting for observation with *Chandra* to observe the X-ray emission morphology, as other massive clusters with Hα emitting BCGs, such as Abell 426 and Abell 1795 show remarkable X-ray morphology, such as X-ray holes, and cooling tails.

ACKNOWLEDGMENTS

We are very grateful to C. Miller and R. Nichol for their help with the SDSS database, and the C4 cluster catalogue. We also thank R. Finn for useful discussions about the C4 clusters. LOVE wishes to thank C. Robert for helpful comments and support during her stay at the University of Waterloo. MJH and MLB acknowledge support from their respective NSERC Discovery grants. We also thank the anonymous referee for a careful reading of the manuscript and useful suggestions.

Table 2. Table of NFPS BCGs. The cluster name is shown in column 1. Column 2 and 3 give the position of the cluster X-ray centre. The cluster redshift is given in column 4, the cluster velocity dispersion and r_{200} are given in columns 5 and 6. Column 7 gives the cooling flow mass deposition rate (MDR) in ($M_\odot$/yr). Column 8 gives the cooling flow status of the cluster. Column 9 gives the reference for the MDR/CF status: b stands for Bîrzan et al. (2004), f for Fujita et al. (2006), j for Johnstone et al. (2005), h for Henry et al. (2004), k for Kempner & David (2004), m for McCarthy et al. (2004), p for Peres et al. (1998), r for Sharma et al. (2004), s for Sanderson et al. (2006), v for Kanov et al. (2006), w for White (2000), and o for other. Column 10 is the X-ray luminosity in units of 10^{44}erg/s, column 11 gives the name of the BCG, column 12 is the BCG K-band magnitude, column 13 gives the distance between the BCG and the cluster X-ray centre. Columns 14 gives the Hβ equivalent width, and column 15 gives the error, which is the noise in the line-free regions of the absorption-corrected spectrum.

Name (Clus)	RA_x (deg)	DEC_x (deg)	z	σ_{cl} (km/s)	r_{200} (Mpc)	MDR ($M_\odot$/yr)	CF	ref	L_X	Name (BCG)	M_K (BCG)	dr (Mpc)	W_oHβ (Å)	Hβ_{err} (Å)
A0085	10.5	-9.3	0.0557	736	1.3	108	✓	p/s	4.920	MCG–02-02-086	-26.0	0.046	1.13	0.21
A0119	14.1	-1.2	0.0436	653	1.1	0	X	p	1.580	UGC-00579	-25.7	0.054	-0.11	0.06
A0133	15.7	-21.9	0.0561	794	1.4	25	X	b/m	1.590	ESO-541–G-013	-25.6	0.017	-0.08	0.09
A0262	28.2	36.2	0.0155	432	0.7	2	✓	b/s	0.230	NGC-0708	-24.8	0.005	1.76	0.06
A0376	41.5	36.9	0.0482	975	1.7	42	X	w	0.680	GIN-138	-24.4	0.408	-0.04	0.06
A0407	45.5	35.8	0.0465	670	1.2	N/A	?	?	0.210	UGC-02489-NED02	-25.6	0.022	-0.14	0.10
A3128	52.6	-52.5	0.0595	838	1.5	N/A	?	?	1.160	2masx-j03295060-5234471	-25.5	0.217	-0.30	0.13
RXJ0341	55.3	15.4	0.0288	502	0.9	N/A	?	?	0.250	2masx-j03412829+1515326	-24.5	0.231	0.04	0.11
A3158	55.7	-53.6	0.0586	814	1.4	292	✓	w	2.820	ESO-156–G-008-NED01	-25.7	0.069	-0.01	0.09
A3266	67.9	-61.4	0.0588	946	1.6	145	X	w/m	3.900	ESO-118-IG-030-NED02	-26.2	0.128	-0.05	0.15
A0496	68.4	-13.2	0.0321	577	1.0	70	✓	o/m	1.770	MCG–02-12-039	-25.5	0.031	1.21	0.18
A3341	81.4	-31.6	0.0376	500	0.9	N/A	?	?	0.310	MCG–05-13-019	-24.9	0.009	-0.01	0.07
A0548A	87.2	-25.4	0.0386	794	1.4	10	X	w	0.370	ESO-488-IG-031	-24.3	0.356	0.20	0.13
A3376	90.4	-40.0	0.0464	710	1.2	0	X	w	1.320	ESO-307–G-013	-25.3	0.470	-0.03	0.06
A3389	95.5	-65.0	0.0270	626	1.1	25	X	w	0.180	NGC-2235	-25.2	0.061	0.13	0.07
A3391	96.6	-53.7	0.0556	696	1.2	131	✓	w	1.370	ESO-161-IG-007-NED02	-26.4	0.055	0.14	0.10
A3395	96.8	-54.5	0.0491	640	1.1	N/A	?	?	1.610	ESO-161–G-008	-25.4	0.158	-0.05	0.12
A0576	110.4	55.8	0.0383	854	1.5	3	X	p/k	0.710	CGCG-261-056-NED01	-25.9	0.008	-0.02	0.05
UGC03957	115.2	55.4	0.0339	511	0.9	N/A	?	?	0.480	UGC-03957	-25.3	0.017	-0.04	0.05
A0602	118.4	29.4	0.0605	675	1.2	N/A	?	?	0.530	2masx-j07532661+2921341	-24.2	0.032	-0.45	0.12
Z1665	125.8	4.4	0.0296	437	0.8	N/A	?	?	0.160	IC-0505	-24.9	0.072	0.02	0.05
A0754	137.3	-9.7	0.0546	784	1.4	218	X	w/h	4.460	2masx-j09083238-0937470	-25.7	0.328	0.06	0.10
A0757	138.4	47.7	0.0514	381	0.7	N/A	?	?	0.460	2masx-j09134460+4742169	-24.5	0.142	-0.01	0.10
A0780	139.5	-12.1	0.0551	641	1.1	492	✓	w/m	3.470	Hydra-A	-25.1	0.015	7.8	0.30
Z2844	150.7	32.7	0.0504	462	0.8	N/A	?	?	0.300	NGC-3099	-25.4	0.048	0.35	0.07
A1367	176.2	19.8	0.0219	747	1.3	0	X	o/m	0.930	NGC-3842	-24.9	0.252	-0.11	0.05
Z4803	181.1	1.9	0.0206	474	0.8	N/A	?	?	0.170	NGC-4073	-25.4	0.000	-0.01	0.05
A1631A	193.2	-15.4	0.0461	531	0.9	N/A	?	?	0.330	2masx-j12523166-1512150	-24.4	0.358	-0.06	0.07
A3528B	193.6	-29.0	0.0547	500	0.9	N/A	?	?	0.690	ESO-443–G-004	-25.8	0.005	-0.14	0.07
A3528A	193.7	-29.3	0.0535	698	1.2	N/A	?	?	1.100	2masx-j12543999-2927327	-24.0	0.482	-0.36	0.25
A3530	193.9	-30.4	0.0544	436	0.8	N/A	?	?	0.380	AM-1252-300-NED02	-25.0	0.018	N/A	N/A
A1656	194.9	27.9	0.0230	898	1.6	85	X	w	3.980	NGC-4889	-25.6	0.169	-0.03	0.03
A1668	195.9	19.3	0.0641	476	0.8	N/A	?	?	0.880	IC-4130	-25.2	0.027	2.39	0.09
A3558	202.0	-31.5	0.0476	814	1.4	235	X	w/s	3.450	ESO-444–G-046	-26.2	0.019	-0.06	0.12
A1736A	201.7	-27.1	0.0465	664	1.2	79	X	w	1.250	IC-4252	-25.8	0.512	-0.02	0.04
A3560	203.1	-33.1	0.0487	548	0.9	N/A	?	?	0.730	2masx-j13322574-3308100	-25.2	0.097	-0.05	0.06
A3571	206.9	-32.9	0.0392	913	1.6	130	X	w/s	3.910	ESO-383–G-076	-26.0	0.022	-0.07	0.14
A1795	207.2	26.6	0.0627	725	1.3	18	✓	b/m	6.330	CGCG-162-010	-25.7	0.016	7.2	0.30
A3581	211.9	-27.0	0.0225	525	0.9	18	✓	w/j	0.320	IC-4374	-24.5	0.003	1.93	0.09
A1983A	223.2	16.7	0.0448	472	0.8	N/A	?	?	0.230	ABELL-1983-1:[CBW93]-C	-24.2	0.050	0.14	0.09
A1991	223.6	18.6	0.0589	454	0.8	37	✓	w/r	0.710	NGC-5778	-25.4	0.023	0.61	0.10
A2052	229.2	7.0	0.0352	531	0.9	81	✓	b/m	1.330	UGC-09799	-25.5	0.038	1.64	0.09
A2063	230.8	8.6	0.0344	764	1.3	99	✓	w/v	1.020	CGCG-077-097	-24.9	0.056	0.10	0.08
A2107	234.9	21.8	0.0415	527	0.9	57	X	w/f	0.570	UGC-09958	-25.5	0.014	-0.18	0.06
A2147	240.6	16.0	0.0370	711	1.2	119	X	w/s	1.660	UGC-10143	-24.9	0.082	-0.02	0.07
A2151A	241.2	17.7	0.0352	746	1.3	173	✓	w	0.430	NGC-6041A	-25.1	0.051	-0.11	0.07
A2199	247.2	39.5	0.0293	647	1.1	2	✓	b/m	1.900	NGC-6166-NED01	-25.7	0.007	2.17	0.11
RXJ1733	263.3	43.8	0.0319	468	0.8	N/A	?	?	0.270	IC-1262	-24.6	0.005	0.35	0.08
RXJ1740	265.1	35.7	0.0434	556	1.0	N/A	?	?	0.270	CGCG-199-007-NED01	-24.9	0.013	-0.12	0.08
Z8338	272.7	49.9	0.0494	532	0.9	N/A	?	?	0.450	NGC-6582-NED02	-25.7	0.098	-0.09	0.04
A3667	303.1	-56.8	0.0549	852	1.5	196	X	w/m	5.020	IC-4965	-25.8	0.700	N/A	N/A
A3716	312.9	-52.7	0.0447	748	1.3	N/A	?	?	0.480	ESO-187–G-020	-25.2	0.098	-0.07	0.08
IIZW108	318.5	2.6	0.0482	399	0.7	N/A	?	?	1.090	IC-1365-NED02	-25.6	0.115	0.04	0.06
A2399	329.3	-7.8	0.0577	608	1.1	N/A	?	?	0.430	2masx-j21572939-0747443	-24.5	0.218	-0.05	0.06
A3880	337.0	-30.6	0.0583	817	1.4	N/A	?	?	0.960	PKS-2225-308	-25.6	0.022	2.94	0.15
Z8852	347.6	7.6	0.0402	771	1.3	N/A	?	?	0.470	NGC-7503	-25.6	0.108	0.08	0.07
A2572B	349.3	18.7	0.0386	138	0.2	N/A	?	?	0.280	NGC-7602	-24.5	0.105	-0.04	0.05
A2589	351.0	16.8	0.0411	583	1.0	0	X	o/m	0.890	NGC-7647	-25.4	0.073	-0.11	0.07
A2634	354.6	27.0	0.0309	692	1.2	0	X	w	0.480	NGC-7720-NED01	-25.5	0.018	0.19	0.08
A4059	359.2	-34.8	0.0496	556	1.0	7	✓	b	1.680	ESO-349–G-010	-26.0	0.019	2.80	0.12

REFERENCES

Abazajian K., Adelman-McCarthy J. K., Agüeros e. a., 2005, AJ, 129, 1755

Allen S. W., Ettori S., Fabian A. C., 2001, MNRAS, 324, 877

Babul A., Balogh M. L., Lewis G. F., Poole G. B., 2002, MNRAS, 330, 329

Baldwin J. A., Phillips M. M., Terlevich R., 1981, PASP, 93, 5

Balogh M. L., Babul A., Voit G. M., McCarthy I. G., Jones L. R., Lewis G. F., Ebeling H., 2006, MNRAS, 366, 624
Best P. N., von der Linden A., Kauffmann G., Heckman T. M., Kaiser C. R., 2006, astro-ph/0611197
Bîrzan L., Rafferty D. A., McNamara B. R., Wise M. W., Nulsen P. E. J., 2004, ApJ, 607, 800
Böhringer H., Matsushita K., Churazov E., Ikebe Y., Chen Y., 2002, A&A, 382, 804
Böhringer H., Schuecker P., Guzzo L., Collins C. A., Voges W., Schindler S., Neumann D. M., Cruddace R. G., De Grandi S., Chincarini G., Edge A. C., MacGillivray H. T., Shaver P., 2001, A&A, 369, 826
Böhringer H., Voges W., Huchra J. P., McLean B., Giacconi R., Rosati P., Burg R., Mader J., Schuecker P., Simiç D., Komossa S., Reiprich T. H., Retzlaff J., Trümper J., 2000, APJS, 129, 435
Bower R. G., Benson A. J., Malbon R., Helly J. C., Frenk C. S., Baugh C. M., Cole S., Lacey C. G., 2006, MNRAS, 370, 645
Brough S., Collins C. A., Burke D. J., Lynam P. D., Mann R. G., 2005, MNRAS, 364, 1354
Carlberg R. G., Yee H. K. C., Ellingson E., 1997, ApJ, 478, 462
Chen Y., Reiprich T. H., Böhringer H., Ikebe Y., Zhang Y. ., 2007, ArXiv Astrophysics e-prints
Condon J. J., Cotton W. D., Greisen E. W., Yin Q. F., Perley R. A., Taylor G. B., Broderick J. J., 1998, AJ, 115, 1693
Crawford C. S., Allen S. W., Ebeling H., Edge A. C., Fabian A. C., 1999, MNRAS, 306, 857
Crawford C. S., Sanders J. S., Fabian A. C., 2005, MNRAS, 361, 17
Croton D. J., Springel V., White S. D. M., De Lucia G., Frenk C. S., Gao L., Jenkins A., Kauffmann G., Navarro J. F., Yoshida N., 2006, MNRAS, 365, 11
De Lucia G., Blaizot J., 2006, astro-ph/0606519
Donahue M., Mack J., Voit G. M., Sparks W., Elston R., Maloney P. R., 2000, ApJ, 545, 670
Ebeling H., Edge A. C., Allen S. W., Crawford C. S., Fabian A. C., Huchra J. P., 2000, MNRAS, 318, 333
Ebeling H., Edge A. C., Bohringer H., Allen S. W., Crawford C. S., Fabian A. C., Voges W., Huchra J. P., 1998, MNRAS, 301, 881
Ebeling H., Voges W., Bohringer H., Edge A. C., Huchra J. P., Briel U. G., 1996, MNRAS, 281, 799
Ebeling H., Wiedenmann G., 1993, Phys. Rev. E, 47, 704
Edge A. C., Wilman R. J., Johnstone R. M., Crawford C. S., Fabian A. C., Allen S. W., 2002, MNRAS, 337, 49
Edwards L. O. V., Robert C., 2007, in Boehringer H. and Schuecker P. and Pratt G.W. and Finoguenov A., eds., ESO Astrophysics Symposia, Heating vs. Cooling in Galaxies and Clusters of Galaxies. Springer-Verlag, Garching
Fabian A. C., 1994, ARA&A, 32, 277
Fujita Y., Sarazin C. L., Sivakoff G. R., 2006, PASJ, 58, 131
Gómez P. L., Nichol R. C., Miller C. J., Balogh M. L., Goto T., Zabludoff A. I., Romer A. K., Bernardi M., Sheth R., Hopkins A. M., Castander F. J., Connolly A. J., Schneider D. P., Brinkmann J., Lamb D. Q., SubbaRao M., York D. G., 2003, ApJ, 584, 210
Hatch N., 2007, in Boehringer H. and Schuecker P. and Pratt G.W. and Finoguenov A., eds., ESO Astrophysics Symposia, Heating vs. Cooling in Galaxies and Clusters of Galaxies. Springer-Verlag, Garching
Henry J. P., Finoguenov A., Briel U. G., 2004, ApJ, 615, 181
Hicks A. K., Mushotzky R., 2005, ApJL, 635, L9
Ho L. C., Filippenko A. V., Sargent W. L. W., 1997, ApJS, 112, 315
Horner D. J., Baumgartner W. H., Gendreau K. C., Mushotzky R. F., 2001, in Two Years of Science with Chandra, Abstracts from the Symposium held in Washington, DC, 5-7 September, 2001, meeting abstract. X-ray Scaling Laws for Galaxy Clusters and Groups
Hudson M. J., Ebeling H., 1997, ApJ, 479, 621
Jaffe W., Bremer M. N., van der Werf P. P., 2001, MNRAS, 324, 443
Johnstone R. M., Fabian A. C., Morris R. G., Taylor G. B., 2005, MNRAS, 356, 237
Johnstone R. M., Fabian A. C., Nulsen P. E. J., 1987, MNRAS, 224, 75
Kanov K. N., Sarazin C. L., Hicks A. K., 2006, ApJ, 653, 184
Kauffmann G., Heckman T. M., Tremonti C., Brinchmann J., Charlot S., White S. D. M., Ridgway S. E., Brinkmann J., Fukugita M., Hall P. B., Ivezić Ž., Richards G. T., Schneider D. P., 2003, MNRAS, 346, 1055
Kempner J. C., David L. P., 2004, ApJ, 607, 220
Kennicutt Jr. R. C., 1998, ARA&A, 36, 189
Laine S., van der Marel R. P., Lauer T. R., Postman M., O'Dea C. P., Owen F. N., 2003, AJ, 125, 478
Lin Y.-T., Mohr J. J., 2004, ApJ, 617, 879
Lin Y.-T., Mohr J. J., 2006, astro-ph/0612521
Lin Y.-T., Mohr J. J., Stanford S. A., 2004, ApJ, 610, 745
Mahdavi A., Böhringer H., Geller M. J., Ramella M., 2000, ApJ, 534, 114
McCarthy I. G., Balogh M. L., Babul A., Poole G. B., Horner D. J., 2004, ApJ, 613, 811
McNamara B. R., O'Connell R. W., 1989, AJ, 98, 2018
McNamara B. R., Wise M., Sarazin C. L., Jannuzi B. T., Elston R., 1996, ApJL, 466, L9+
McNamara B. R., Wise M. W., Murray S. S., 2004, ApJ, 601, 173
Miller C. J., Nichol R. C., Reichart D., Wechsler R. H., Evrard A. E., Annis J., McKay T. A., Bahcall N. A., Bernardi M., Boehringer H., Connolly A. J., Goto T., Kniazev A., Lamb D., Postman M., Schneider D. P., Sheth R. K., Voges W., 2005, AJ, 130, 968
Mulchaey J. S., Zabludoff A. I., 1998, ApJ, 496, 73
Nelan J. E., Smith R. J., Hudson M. J., Wegner G. A., Lucey J. R., Moore S. A. W., Quinney S. J., Suntzeff N. B., 2005, ApJ, 632, 137
Peres C. B., Fabian A. C., Edge A. C., Allen S. W., Johnstone R. M., White D. A., 1998, MNRAS, 298, 416
Peterson J. R., Kahn S. M., Paerels F. B. S., Kaastra J. S., Tamura T., Bleeker J. A. M., Ferrigno C., Jernigan J. G., 2003, ApJ, 590, 207
Pizzolato F., Soker N., 2005, ApJ, 632, 821
Popesso P., Böhringer H., Brinkmann J., Voges W., York D. G., 2004, A&A, 423, 449
Rafferty D. A., McNamara B. R., Nulsen P. E. J., Wise M. W., 2006, ApJ, 652, 216
Sadat R., Blanchard A., Kneib J.-P., Mathez G., Madore

B., Mazzarella J. M., 2004, A&A, 424, 1097
Salomé P., Combes F., 2003, A&A, 412, 657
Sanderson A. J. R., Ponman T. J., O'Sullivan E., 2006, MNRAS, 372, 1496
Scott E. L., 1957, ApJ, 62, 248
Sharma M., McNamara B. R., Nulsen P. E. J., Owers M., Wise M. W., Blanton E. L., Sarazin C. L., Owen F. N., David L. P., 2004, ApJ, 613, 180
Sijacki D., Springel V., 2006, MNRAS, 366, 397
Silk J., Rees M. J., 1998, A&A, 331, L1
Skrutskie M. F., Cutri R. M., Stiening R. e. a., 2006, AJ, 131, 1163
Smith R. J., Hudson M. J., Nelan J. E., Moore S. A. W., Quinney S. J., Wegner G. A., Lucey J. R., Davies R. L., Malecki J. J., Schade D., Suntzeff N. B., 2004, AJ, 128, 1558
Stoughton C., Lupton R. H., Bernardi e. a., 2002, AJ, 123, 485
Strateva I. I. Ž., Knapp G. R. e. a., 2001, AJ, 122, 1861
Vazdekis A., 1999, ApJ, 513, 224
von der Linden A., Best P. N., Kauffmann G., White S. D. M., 2006, astro-ph/0611196
White D. A., 2000, MNRAS, 312, 663
White R. L., Becker R. H., Helfand D. J., Gregg M. D., 1997, ApJ, 475, 479